Chapter-6

6 Fluorometric based detect of organic pollutant of para nitrophenol (PNP) using boron nitrate quantum dots (BNQDs) with high selectivity and sensitivity

6.1 Introduction

In recent decades, the release of organic contaminants into the atmosphere and water resources has posed a serious threat to the ecology[311]. Nitroaromatic chemicals, which are widely used in various industries, have contributed to the pollution of natural ecosystems, including waterways and soil treated with pesticides or herbicides[312], [313]. Para-nitrophenol (PNP) is harmful to the environment because it is toxic to aquatic life and can accumulate in the food chain. It can also have negative effects on plant growth and reproduction. PNP is classified as persistent bio-accumulative and toxic chemical, meaning that it remains in the environment for long time, builds up in the bodies of living organisms, and is toxic at low levels. PNP has been identified as a priority pollutant by the US Environmental Protection Agency (EPA), US Food and Drug Administration draught, and European Medicines Agency and is subject to regulation under the Clean Water Act[314]–[316]. Para-nitrophenol (PNP) is a toxic organic compound that is widely used in the manufacture of various chemicals, and dyes. PNP is also released by the leather[317], textile[318], iron and steel[319], foundry[320], rubber sectors[321], and pharmaceutical[322] as well as the fabrication of electrical and electronic components[318]. It can be released into the air, water, and soil through various anthropogenic activities, such as industrial effluents, agricultural runoff, and domestic wastewater[323], [324]. PNP is also have high stability and high solubility in water and clay soil[325], [326]. Therefore, Short-term exposure to PNP can cause various health issues such as kidney and liver damage, central nervous system dysfunction, headaches, skin rashes, cyanosis, methemoglobinemia, drowsiness, and nausea[326], [327].

Recent research has highlighted the adverse impacts of p-nitrophenol (PNP) on animals, including endocrine disruption and reproductive interference[328], [329]. Studies have shown that PNP is recalcitrant and difficult to degrade, leading to the formation of hazardous nitroso and hydroxylamine derivatives upon reduction by reductases[330]–[333]. Although certain bacteria in nature can modify or degrade nitrophenols[334], their efficacy is limited, and there is a need for alternative detection strategies to monitor PNP levels in environmental samples. Given the potential harm associated with PNP, the development of sensitive and selective detection methods has received significant attention in recent years. Various techniques, such as electrochemical sensors, colorimetric assays, and fluorescence-based assays, have been explored for the detection of PNP[335]–[337]. These methods offer advantages such as high sensitivity, specificity, and real-time monitoring capabilities, making them promising tools for environmental monitoring[338], [339]. However, Various techniques, including gas chromatography[340], liquid chromatography[341], capillary electrophoresis[342], fiber optode[343], electrochemical[344], [345] and UV-Vis spectrophotometry[346], have been used to detect PNP. In recent years, fluorescence-based detection has gained significant attention due to its simplicity, high sensitivity, selectivity, small response time, and low cost compared to other analytical techniques[347], [348]. However, the application of some existing fluorescence probes is limited due to their complexity of pre-treatments, low selectivity, and high instrument costs. To overcome these limitations, researchers have developed numerous fluorescence-based techniques using a range of materials, including conjugated polymers[349], [350], metal-organic frameworks (MOFs)[351], [352], nitrogen-doped carbon nanodots[353], [354], and others.

Although several fluorescence probes have been developed for the detection of various analytes, most of them require expensive materials or time-consuming production

techniques[348]. For example, molecularly imprinted polymers (MIPs) and non-imprinted polymers (NIPs) coated graphene quantum dots have been used as fluorescence probes for the detection of p-nitrophenol (PNP), but their production is time-consuming[355]. Therefore, developing efficient and inexpensive strategies for the quantitative and qualitative determination of PNP is an urgent need.

In this study, we have synthesized a Quantum dot by using one step hydrothermal process with precursor as boron nitride with citric acid as stabilizer as well as nitrogen dopant, which have water dispersible and give blue-green broad emission with absolute quantum yield (QY = 5.4%). The synthesized nanodots have good optical properties with excellent pH, ionic and storage time stability. It can recognize PNP by fluorometric sensing quickly and effectively.

6.2 Result and Discussion

6.2.1 Optical Characterization of the Synthesized Materials

The UV-Vis absorption spectra of synthesized materials, both with and without hydrothermal treatment, have been investigated and distinct absorption bands have been observed. In Figure 6.1(a), it is observed that without hydrothermally treated BN (WH-BN), a broad and weak absorption peak is present at 240-300nm, which is attributed to the n- π * transition. Furthermore, the UV-Vis absorption spectra of pure PNP and WH-BN precursor with PNP were also recorded, and two absorption bands were observed in the case of pure PNP at 235nm and 260-450nm. In the case of WH-BN with PNP, absorption at 235nm and 260-400nm was also observed. The absorption band corresponding to 235nm is attributed to the C=O bond and contributed n- π * transition, whereas the absorption band at 260-450nm is attributed to the C=C bond and π - π * transitions[169].

In the case of hydrothermally treated BN (BNQDs), as shown in Figure 6.1(b), an absorption band at 245nm was observed, which is attributed to the n- π * transition. The absorption behavior of PNP and BNQDs with PNP was found to be like that of Figure 6.1(a). These findings suggest that hydrothermal treatment affects the UV-Vis absorption spectra of BN and its precursor with PNP, resulting in changes in absorption bands and peak intensities. The observed absorption bands can be attributed to specific electronic transitions, which provide important information about the molecular structure and properties of the synthesized materials. In Figure 6. 1(c, & d), the tau plots of WH-BN and BNQDs were presented, and the corresponding band gaps were determined to be 5.48 eV and 5.53 eV, respectively.

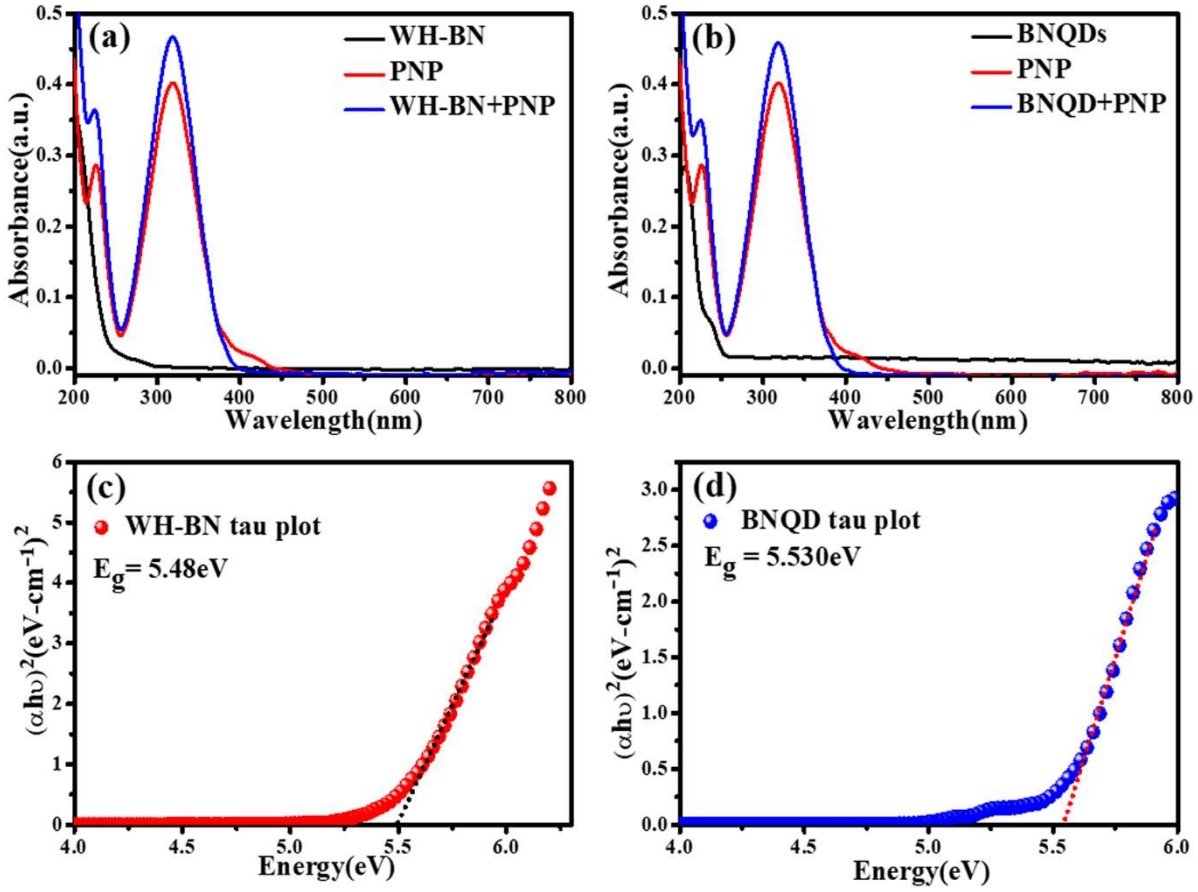

Figure 6. 1 (a) UV-VIS absorption spectra of WH-BN, PNP and WH-BN+PNP, (b) UV-Vis absorption spectra of synthesized BNQDs, PNP and BNQDs + PNP, (c) Tau plot of WH-BN, (d) Tau plot of synthesized BNQDs

Figure 6.2(a) shows the Fourier transform infrared spectroscopy (FTIR) spectra of synthesized BNQDs, PNP and BNQDs + PNP were analyzed to identify the presence of surface functional groups. The observed O-H and N-H stretching vibrations at 3429 cm^{-1} and weak absorption at 2922 cm^{-1} corresponded to C-H stretching[356], respectively. The medium absorption peak at 1640 cm^{-1} indicated the presence of C=C or aromatic ring stretching[55], while the C-O stretching band appeared at 1160 cm^{-1}. The stretching mode at 1060 cm^{-1} corresponded to C-O-C and C-N vibration mode.

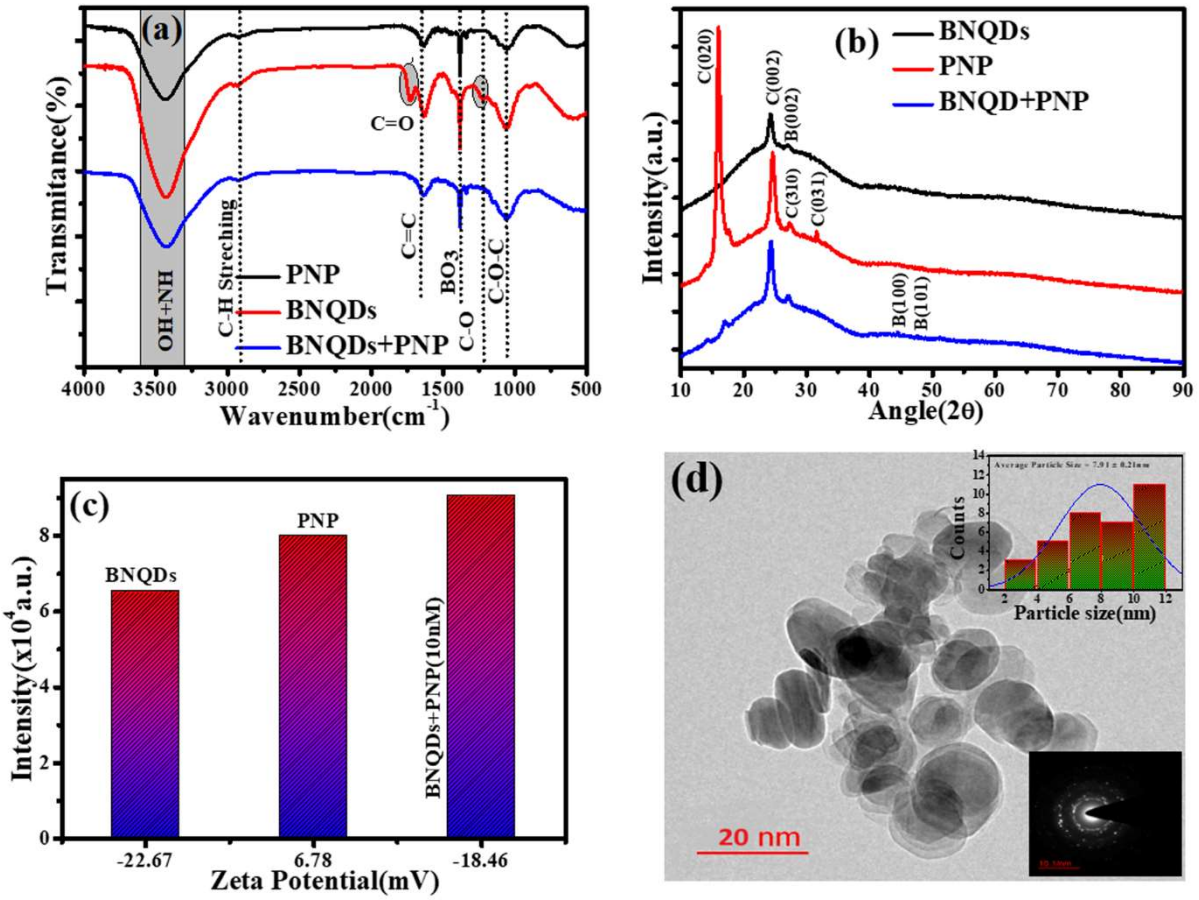

Figure. 6. 2 (a) FTIR spectra of PNP, BNQDs, and BNQDs + PNP, (b) XRD spectra of the BNQDs, PNP, and BNQDs + PNP, (c) Zeta potential of BNQDs, PNP, and mixed of BNQDs +PNP, (d) XPS survey spectra of BNQDs, PNP, and BNQDs +PNP.

These vibrations were observed in all samples, but in BNQDs, additional absorption peaks were found at 1727 and 1225 cm^{-1}, corresponding to C=O and C-N stretching bands, respectively, as well as a BN stretching absorption band appear at 1440, 1634 cm^{-1}[357], [358]. These results indicate that the surface of BNQDs is decorated with functional groups and that they interact with PNP. The X-ray diffraction (XRD) pattern of Boron Nitride Quantum Dots (BNQDs), PNP, and their mixture was analysed in Figure 6.2(b). The pattern revealed a mixture of amorphous and crystalline phases in all three samples. The BNQDs exhibited the presence of C(002) and B(002) crystalline phases at 24.35º and 27.07º, respectively. Conversely, the PNP sample showed the presence of C(110), C(002), C(200), and C(120) crystal planes at 15.96º, 24.35º, 27.36º, and 31.62º, respectively. The mixing of BNQDs and PNP resulted in a change in the crystal structure, indicating interaction between the two materials. The mixture showed the appearance of C(110), C(002), B(002), B(100), and B(101) crystal planes at 15.96º, 24.35º, 27.07º, 44.49º, and 47.58º[359], [360], respectively. Figure 6.2(c) depicted the zeta potential of BNQDs, PNP, and their mixture. The surface potential charge of the BNQDs was found to be -22.67±0.2mV, whereas that of pure PNP was 6.78±0.2mV. Since BNQDs and PNP exhibited opposite charges, the possibility of strong interaction between them was observed after mixing. The zeta potential of the BNQDs +PNP mixture was found to be -18.46±0.2mV, indicating the interaction between the two materials. Figure 2(d) depicts a TEM image of BNQDs, providing information on their shape and size. The BNQDs were observed to have a spherical shape upon synthesis, and their size was determined through analysis using Image J software, yielding an average particle size of 7.91 ± 0.21 nm as shown in the inset of Figure 6.2(d). Additionally, the sample's crystallinity, lattice parameters, and crystal structure were evaluated through the SAED image also presented in the inset of Figure 6.2(d).

Figure 6.3(a) shows the high-resolution XPS photoelectron peaks of C1s in the range of 280 to 292eV for BNQDs, PNP, and BNQDs + PNP. The mixed BNQDs + PNP sample exhibited different photoelectron spectra with respect to BNQDs, indicating the formation of new functional groups.

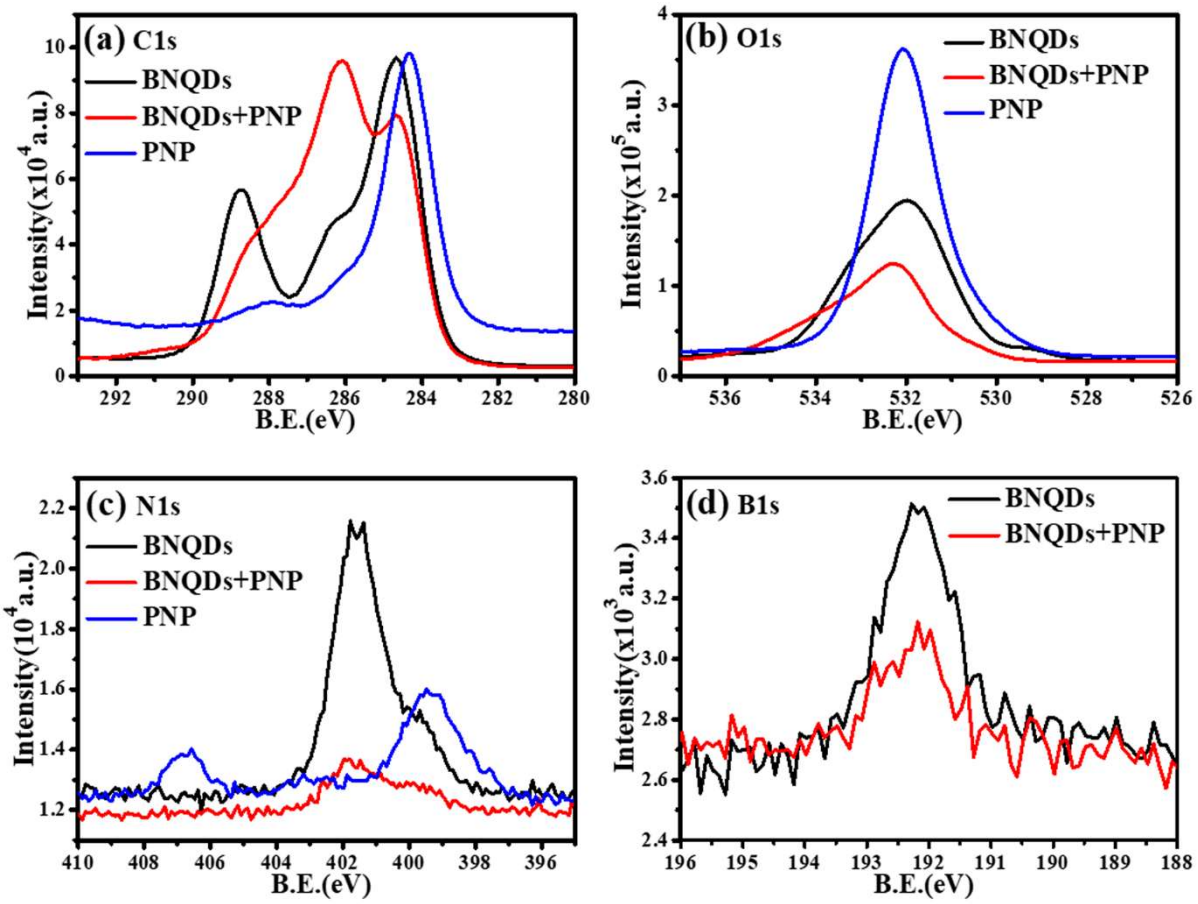

Figure 6. 3 (a, b, & c) High resolution XPS photoelectron peaks of C1s, O1s, and N1s of the BNQDs, PNP, and BNQDs + PNP. (d) High resolution XPS photoelectron peaks of B1s of the BNQDs, and BNQDs + PNP.

The area percentage of the presence of functional groups change was also observed. In Figure 6.3(b), the O1s peaks of BNQDs, PNP, and BNQDs + PNP were observed at the same position but with different intensities, suggesting significant changes in the area percentage of the presence of functional groups. The O1s XPS spectra were recorded in the range of 526 to

537eV. Similarly, the high-resolution photoelectron XPS spectra of N1s for BNQDs, PNP, and BNQDs + PNP were recorded in the range of 395 to 410eV, as shown in Figure 6.3(c). The intensity and position of the N1s photoelectron peak of PNP were shifted, providing information about the interaction. The XPS spectra of B1s in BNQDs and BNQDs + PNP were recorded and illustrated in Figure 6.3(d). The B1s peaks were observed at the same position, but changes occurred in intensity. The XPS survey spectrum of BNQDs, PNP, and BNQDs + PNP exhibited characteristic peaks, and their atomic percentages of C1s, O1s, and N1s were tabulated in Table 6.1.

Peak Table	BNQDs		PNP		BNQDs + PNP	
	Position (eV)	**% Atomic**	**Position (eV)**	**% Atomic**	**Position (eV)**	**% Atomic**
C1s	293.08-277.08	58.76	291.58-278.58	40.58	293.08-277.08	73.06
O1s	538.08-523.08	38.55	539.08-523.08	58.1	538.58-524.08	25.77
N1s	406.08-395.08	2.27	408-394	1.32	406.58-391.08	1.10
B1s	194-182	0.42	1307-1298	-	194-182	0.07

Table 6. 1 The C1s, O1s, N1s, and B1s peak positions and their atomic percentage of the synthesized BNQDs, PNP, and BNQDs + PNP.

It can be concluded that the atomic percentage of C1s increases with the addition of PNP, while the atomic percentage of O1s decreases. A minor change is also observed in the atomic percentages of N1s and B1s.

The complementary use of FTIR and XPS techniques can provide valuable information about the chemical and structural properties of materials, and can be used to confirm the presence of certain functional groups on their surface. The surface chemistry of boron nitride quantum dots

(BNQDs), PNP, and their mixture was investigated using X-ray photoelectron spectroscopy (XPS). Figure 6.4(a, &b) illustrate that, the C1s deconvolution of the BNQDs showed the presence of functional groups O-C=O, C=O, C-O/C-N, C=C/C-C, and C-H at 288.77 eV, 287.70 eV, 286.42 eV, 284.60 eV, and 285.47 eV, respectively. Similarly, the PNP exhibited O-C=O, C=C/C-C, and C-H functional groups at 288.05 eV, 284.31 eV, and 285.78 eV, respectively. The XPS analysis of the mixture of BNQDs and PNP revealed the presence of functional groups O-C=O, C=O, C-O/C-N, and C=C/C-C at 288.78 eV, 287.75 eV, 286.05 eV, and 284.53 eV,[55], [357] respectively, shown in Figure 6.4(c). These findings suggest that the addition of PNP to BNQDs induces changes in their surface chemistry due to the interaction and formation of complexes between these two materials.

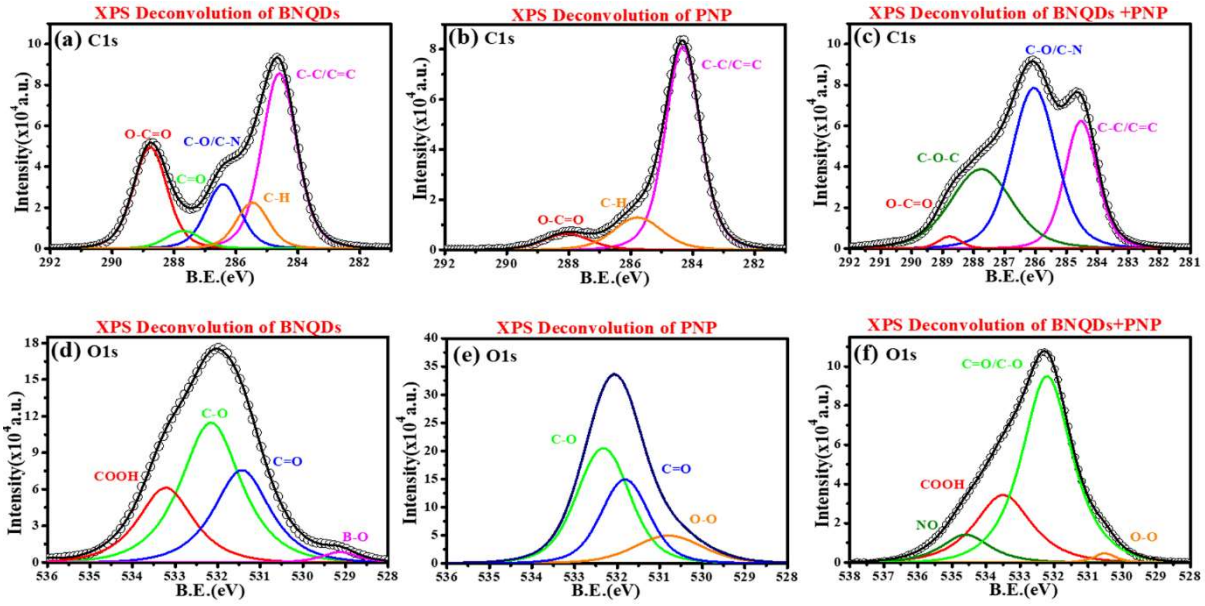

Figure 6. 4 (a, b, & c) C1s deconvolution of BNQDs, PNP, and BNQDs + PNP, (d, e, & f) shows the XPS photoelectron deconvolution of O1s BNQDs, PNP, and BNQDs + PNP.

In Figure 6.4(d, e, &f), the O1s X-ray photoelectron spectroscopy (XPS) data of BNQDs, PNP, and BNQDs + PNP were deconvoluted to identify the functional groups present on their surfaces. Figure 6.5(a) displays the high-resolution X-ray photoelectron spectroscopy (XPS)

survey spectra of BNQDs, PNP, and BNQDs + PNP in the energy range of 0eV to 1350eV, where C1s, O1s, N1s, and B1s photoelectron peaks were observed. The deconvolution of BNQDs revealed the presence of four functional groups, namely COOH, C-O, C=O, and B-O, with binding energies of 533.21eV, 532.13eV, 531.43eV, and 529.10eV, (Figure 6.5 (b & c) respectively. For PNP, three functional groups were identified, including C-O, C=O, and O-O, with binding energies of 532.45eV, 531.87eV, and 530.51eV, respectively. The BNQDs + PNP mixture exhibited four functional groups, including N-O, COOH, C-O/C=O, and O-O, with binding energies of 534.63eV, 533.47eV, 532.17eV, and 530.49eV (Figure 6.5 (d-f)) [55], [357], [361]respectively.

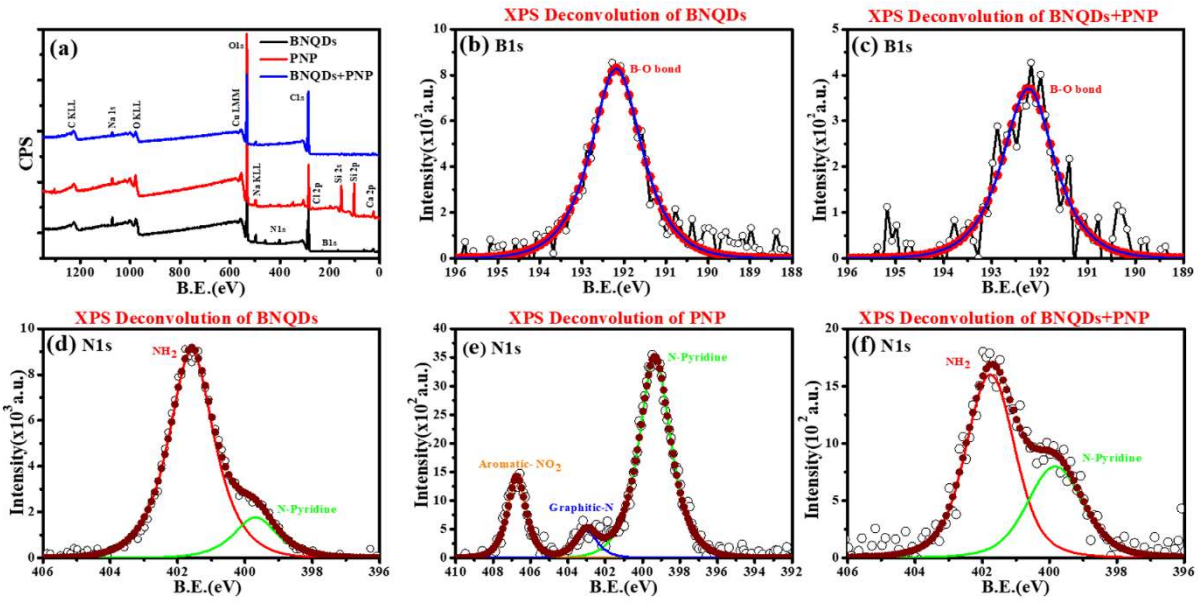

Figure 6. 5 Deconvolution of XPS spectra, (a) High resolution of photoelectron XPS spectra recorded between 0 to1350eV, (b, &c) shows the deconvolution of B1s photoelectron XPS spectra of BNQDs with and without PNP, (d-f) shows the deconvolution of N1s of BNQDs, PNP, and BNQDs + PNP.

The presence of the N-O functional group in the BNQDs + PNP mixture may be attributed to the interaction between the nitrogen-containing PNP and the surface of BNQDs. These results

offer insights into the surface chemistry of the materials, which is essential for comprehending their properties and potential applications.

6.2.2 Sensitivity and Selectivity of Para Nitro Phenol (PNP)

The sensing capabilities of boron nitride quantum dots (BNQDs) were investigated using photo luminescence measurements. In order to detect the presence of p-nitrophenol (PNP), The BNQDs synthesized at 180ºC with a concentration of 0.05µg/mL were employed for selective detection. The selectivity of PNP emission in comparison to various cariogenic heavy metal ions including Cd^{2+}, K^{+}, Zn^{2+}, As^{3+}, NH^{4+}, Hg^{2+}, Fe^{3+}, Pb^{2+}, Na^{+}, and F^{-} was investigated and the results are depicted in Figure 6.6(a). We observed that there were no significant changes in the PL intensity of the BNQDs after addition of metal ions. The excitation wavelength was set at 340nm and the emission spectra were observed at 425nm. Figure 6.6(b) presents the bar diagram of PNP selectivity in the presence of different metal ions. The results demonstrate that BNQDs have high selectivity towards PNP and could be employed for the detection of this compound in various environmental samples. However, we have also investigated the selectivity of BNQDs towards p-nitrophenol (PNP) as a potential detection method. We have also examined the selectivity of PNP compared to similar structured molecules such as aminophenol, methyl phenol, di nitro benzene, phenol, and aniline (Figure 6.6(c)). The PL selectivity measurements were conducted at a concentration of 100µM and the same excitation wavelength (340nm). Our results indicated that PNP detection using BNQDs is highly selective as no significant changes were observed with the similar structured molecules. The bar diagram in Figure 6.6(d) illustrates the PNP selectivity compared to the other analytes. In the bar diagram F_o represents the PL intensity of the control sample corresponding 425nm, which is a diluted BNQDs sample, while F represents the PL intensity of BNQDs with different concentration of analyte. Our highly sensitive detection of PNP is demonstrated by the fact

that, as shown in Figure 6.6, the PNP fully suppresses the PL emission. We conclude as, our findings suggest that BNQDs could be a promising Synthesized material for the highly selective and sensitive detection of PNP.

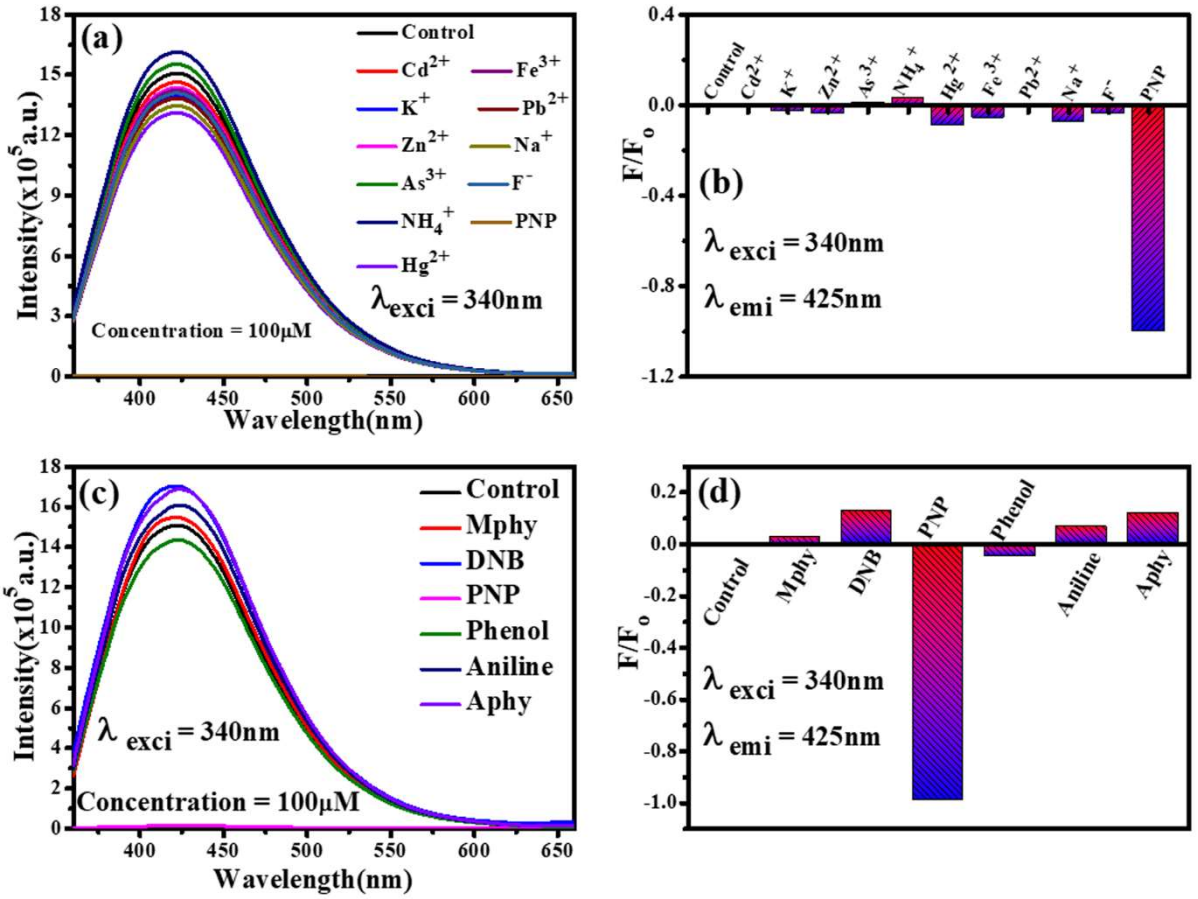

Figure 6. 6 (a) PL emission spectra of control (BNQDs) and BNQDs with different metal ions by using excitation wavelength 340nm, (b) Bar diagram of the PNP detection with respect to different metal ions, (c) PL emission spectra of control (BNQDs) and BNQDs with different PNP type similar molecules by using excitation wavelength 340nm, (d) Bar diagram of the PNP detection with respect to similar molecules.

We have also examined the stability of BNQDs on the basis of pH, UV, salinity, and storage. To obtained the good result over the stability shown in Figure 6.7.

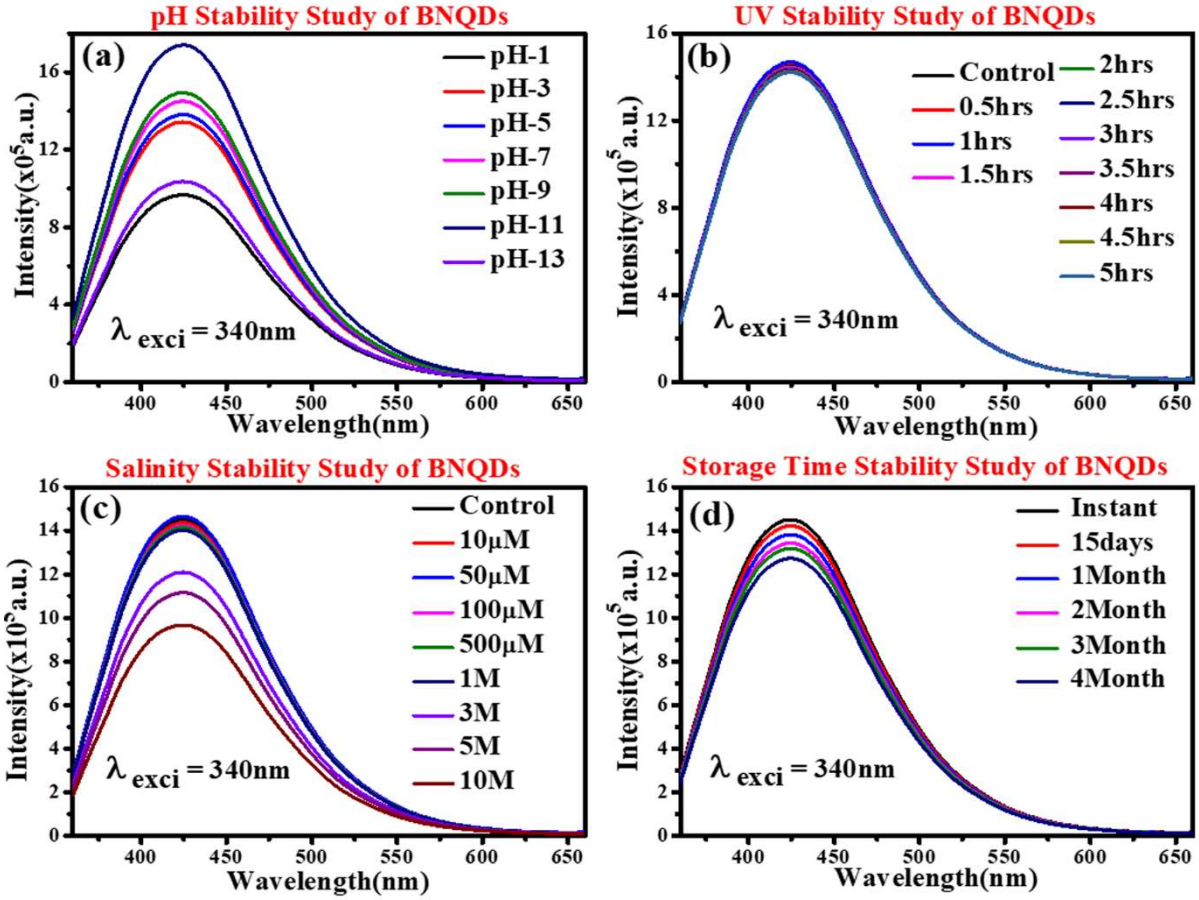

Figure 6. 7 PL emission Stability study of BNQDs, (a) Study of PL emission stability at different pH value, (b) PL emission stability of BNQDs in the presence of exposing UV light at different times, (c) PL emission stability of BNQDs at different concentration of salinity, (d) shows the time of sample storage study of BNQDs.

6.2.3 Sensing of Para Nitro Phenol (PNP)

To investigate the photoluminescence (PL) quenching of as-synthesized boron nitride quantum dots (BNQDs) with the addition of p-nitrophenol (PNP), we conducted experiments shown in Figure 6.8(a). Our results in Figure 6.8(b) indicate that the quenching phenomena is complex and non-linear. The inset of Figure 6.8(b) shows that the Stern-Volmer (S-V) plot exhibits an approximately linear range of 0.1nM to 1μM of PNP concentration. Using the S-V plot, we obtained a linear equation and correlation coefficient of Y = -0.05651X-0.00372 and 0.995, respectively. Furthermore, we used the limit of detection (LOD) formula (equation 2) to

calculate the LOD, which was determined to be 7.91pM. Our results indicate that the LOD obtained is much better than previously reported work for the detection of PNP. A summary of various performance parameters, including LOD, sensitivity, and selectivity, has been provided in Table 6.2 for comparison with the reported work.

Materials	**Based On**	**Linear range**	**LOD**	**Ref.**
N-GQDs	Fluorometric	0–20μM	0.29μM	[362]
Cr-CDs	Fluorometric	0.8-150 μM	0.27μM	[363]
N,Si-CDs	Fluorometric	-	0.011μM	[364]
B-CD-CQD	Fluorometric	10-110μM	0.7μM	[365]
Paper based analytical device	electrochemical	10-200μM	1.1μM	[366]
Polypyrrole-sodium dodecyl sulphate film	electrochemical	0.1-100μM	0.1nM	[367]
Our work	Fluorometric	100pM-1μM	7.91pM	

Table 6. 2 Table comparing the LOD limit of PNP detection using different active sensing material.

Thus, the quenching of PL emission intensity can be attributed to a variety of processes which include dynamic and static quenching. Static quenching occurs when the fluorophore forms a non-fluorescent complex with a quencher molecule. The quencher molecule can be any molecule that can interact with the fluorophore and take up the energy that the fluorophore would have emitted as fluorescence. This interaction is typically due to a strong, long-range interaction such as electrostatic interactions, hydrogen bonding, or Vander Waals forces[137]. In static quenching, the complex between the fluorophore and the quencher molecule is formed before the excitation of the fluorophore. As a result, the complex does not emit fluorescence.

The complex can also be formed in the excited state, which leads to a reduction in the fluorescence intensity. The rate of static quenching is proportional to the concentration of the quencher molecule. Dynamic quenching occurs when the fluorophore interacts with a quencher molecule in the excited state. This interaction can occur via a short-range collisional mechanism such as diffusion-controlled quenching or energy transfer. In dynamic quenching, the excited state fluorophore transfers energy to the quencher molecule, which results in a decrease in fluorescence intensity.

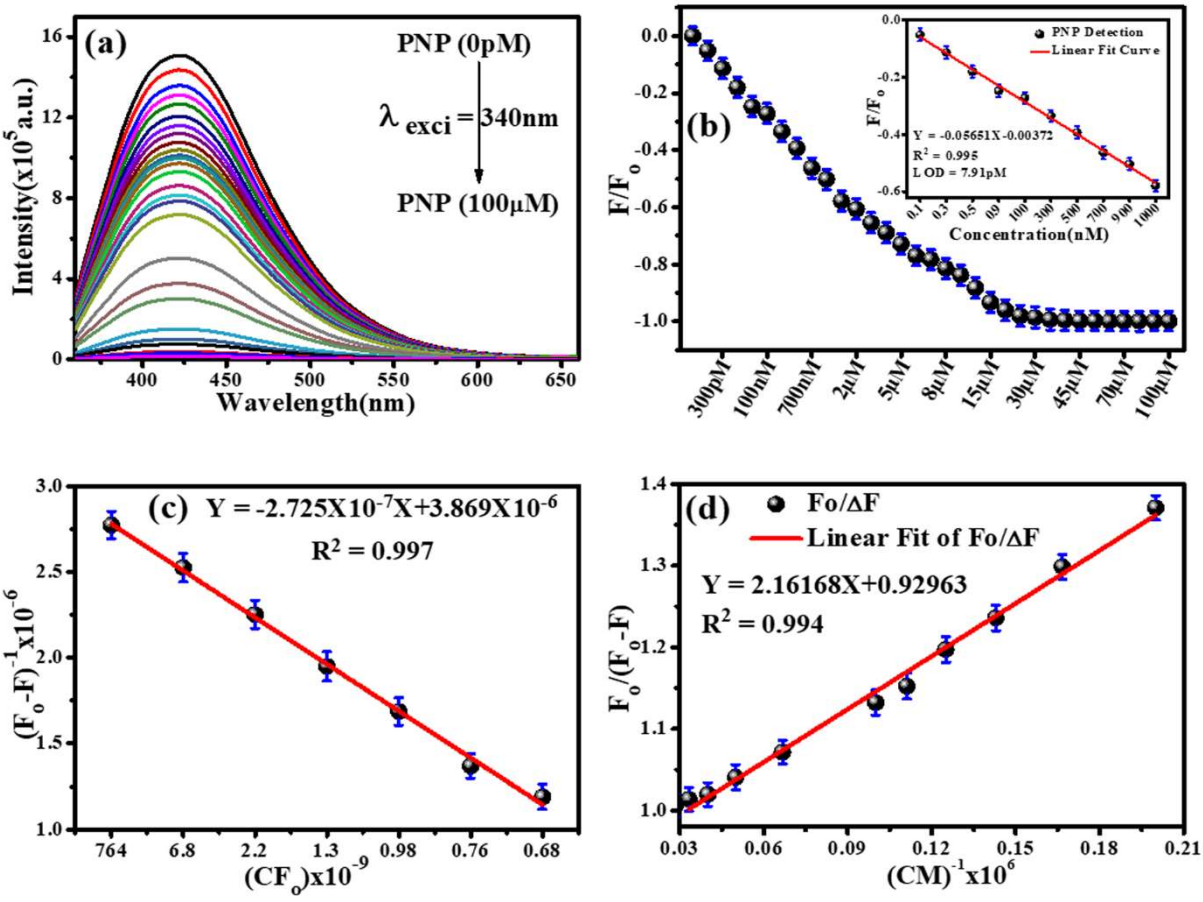

Figure 6. 8 (a) PL emission spectra of BNQDs with different concentration of PNP (0pM-100μM), (b) Stern-Volmer plot, inset shows the linear fitting in the range 0.1nM to1μM, (c) Lineweaver-Burk plot of PL quenching with the addition of different concentration of PNP, (d) Modified S-V plot for the sensing of PNP.

The rate of dynamic quenching depends on the rate of collision between the fluorophore and the quencher molecule, the efficiency of energy transfer, and the concentration of the quencher molecule. Dynamic quenching is generally faster than static quenching because it occurs during the excited state lifetime of the fluorophore. Furthermore, to understand the static and dynamic quenching processes involved, the Lineweaver-Burk equation (L-B) have been plotted with equation 6.1[368], [369].

$$\frac{1}{F - F_o} = \frac{1}{F_o} + \frac{K_m}{F_o C_q} \quad \ldots\ldots\ldots\ldots\ldots\ldots\ldots\ldots\ldots\ldots (6.1)$$

Where F_o and F represent the intensity in the absence and presence of PNP, K_m is Lineweaver-Burk quenching constant and C_q represent the concentration of quencher.

To gain insight into the kinetics of fluorescence quenching, we plotted a graph between 1/(Fo-F) and concentration, which was also plotted in concurrence with the double reciprocal plot or Lineweaver-Burk plot using equation 3 as shown in Figure 6.8(c). Our linear fitting of the data resulted in a correlation coefficient (R^2) of 0.997 and a linear equation of $Y = -2.725x10^{-7}X+3.869x10^{-6}$. From this linear equation, we obtained a K_m value of 3.86μM, which suggests that BNQDs have a strong affinity towards complex formation with PNP. A small amount of BNQDs is required to achieve the given rate, and therefore, even lower concentrations of PNP solutions can be detected using the proposed sensing probe[370]. So, for a better understanding of the complex quenching phenomenon, a modified S-V plot has been in figure 6.8(d), followed by the equation 6.2[137].

$$\frac{F_o}{F_o - F} = \frac{1}{F_a} + \frac{1}{f_a K_a C_q} \quad \ldots\ldots\ldots\ldots\ldots\ldots\ldots\ldots\ldots\ldots (6.2)$$

Here F_o and F is the intensity in the absence and presence of quencher (PNP), To further demonstrate the effectiveness of the quencher in reducing the PL intensity, a modified Stern-Volmer (S-V) plot was constructed, and the parameters f_a and f_aK_a were extracted from it. The values of f_a^{-1} and $(f_aK_a)^{-1}$ were found to be 0.929 and 2.16M, respectively.

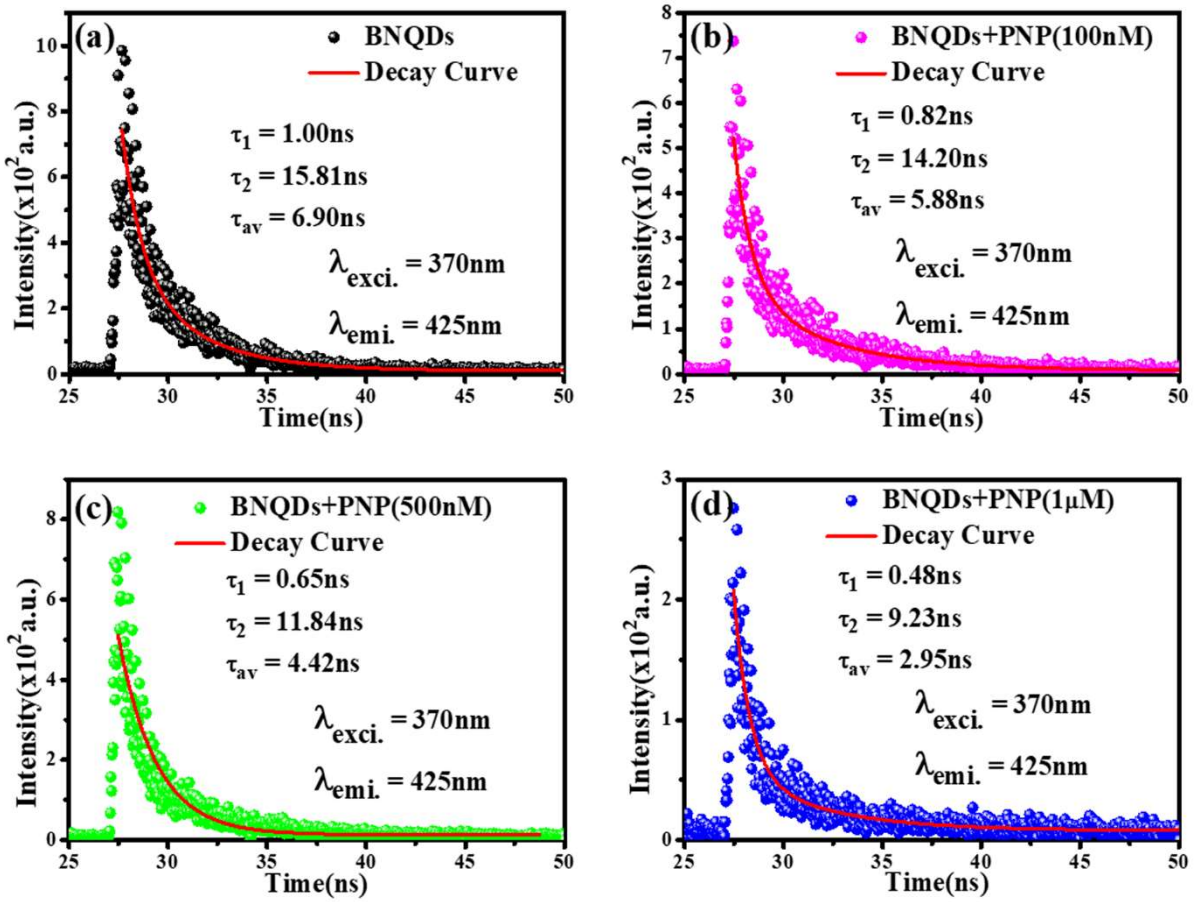

Figure 6. 9 (a- d) TRPL spectra of as synthesized materials BNQDs with and without PNP at different concentration (100nM, 500nM, and 1μM) with correlation coefficient (R2 = 0.992), excitation and emission fixed at 370nm and 425nm.

These values indicate that a significant portion of the initial PL intensity has been quenched by the addition of the quencher. the value of K_a was determined to be $2.325M^{-1}$, which is 14.49% of the collision quenching phenomena derived constant. This suggests that the quenching by the quencher towards the BNQDs PL intensity is a defined process that is different from the

collision quenching phenomena. Furthermore, the quite sensitive technique TRPL spectroscopy is used to examine the dynamic and static quenching processes. Using fixed excitation and emission values of 370 nm and 425 nm, respectively, we are measuring lifetime with and without the addition of PNP, as shown in Figure 6.9(a-d). The average lifetime of as-produced BNQDs decays from 6.9 to 2.95 nanoseconds. The second order exponential decay given in the equation has been found to best fit the data from the TRPL decay investigation using the appropriate software (equation 6.3)[137].

$$y = A_1 e^{-t/\tau_1} + A_2 e^{-t/\tau_2} \quad \ldots\ldots\ldots\ldots\ldots\ldots\ldots\ldots\ldots\ldots\ldots\ldots (6.3)$$

It illustrates the involvement of two different quenching species in PL quenching and shows good agreement with S-V plot analysis. It has been noted that the lifetimes τ_1 and τ_2 decline from 1ns to 0.78ns and 15.81ns to 9.23ns, respectively. Figure 6.10(a) displays the average linear plot with the gradually addition of PNP. The quenching-related data that were attained have been summarised in Table 6.3.

Conc. PNP (nM)	**τ_1(ns)**	**τ_2(ns)**	**τ_{av}(ns)**	**τ_o/τ_{av}**
0	1	15.81	6.9	1
100	0.82	14.2	5.88	1.17
500	0.65	11.84	4.42	1.56
1000	0.48	9.23	2.95	2.33

Table 6. 3 Decay time of BNQDs in presence of different concentration of PNP.

The calibration plot (Figure 6.10(b)) for variables τ_1 and τ_2 has been followed by the equation6.4[137].

$$\frac{\tau_0}{\tau} = 1 + K_q\tau_o(Q) \;=\; 1 + K_D(Q) \;\ldots\ldots\ldots\ldots\ldots\ldots (6.4)$$

Here K_q, τ_o, τ, K_D, and Q represent a biomolecular quenching constant, a lifetime of BNQDs without and with the addition of quencher and S-V constant, respectively.

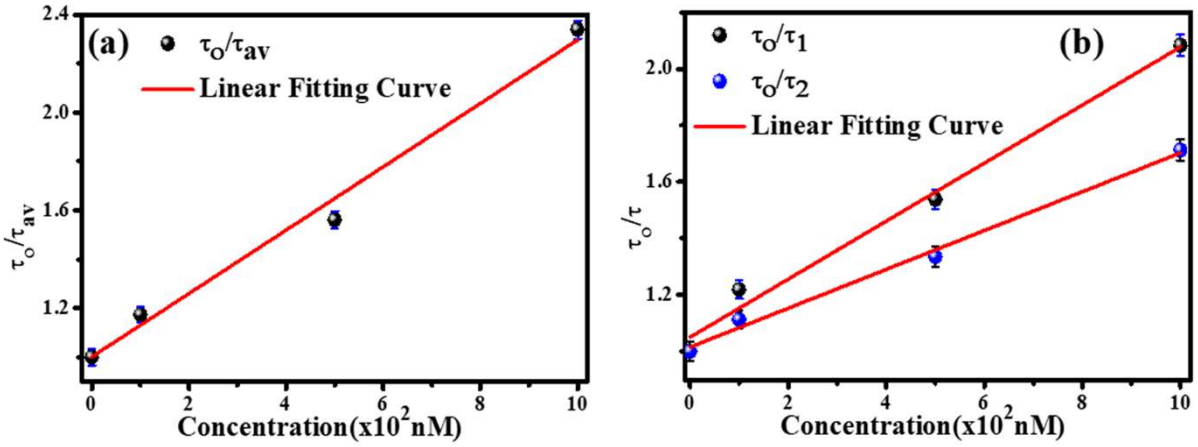

Figure 6. 10 Plot of lifetime ratio plot of BNQDs with addition of PNP, (a) shows the average lifetime decay curve, (b) calibration plot of lifetime decay for τ_1 and τ_2.

The calculated value of K_D ($2.5x10^6$M) showed that 500nM of PNP would be needed to quench the PL emission intensity of CQDs by 19%. On the other hand, the value of K_q $4.95x10^5$ $M^{-1}s^{-1}$ indicates the selection of BNQDs for PNP sensing to be extremely sensitive and effective.

6.2.4 The Mechanism for PL Quenching

The PL intensity has significantly decreased, as seen in the PL emission and TRPL spectra, and the addition of the quencher to the solution has also significantly altered the BNQDs and decay lifespan. As a result, there has been a definite indication of PL quenching caused by both collisional and static quenching. This may be due to the presence of different functional groups on the surface of as synthesized BNQDs. FTIR and XPS measurements are used to identify these functional groups. Table 6.4(a, &b) lists all the species present in C1s and O1s, along

with their peak positions and area percentages. Graphitic carbon makes up roughly 59% of BNQDs as synthesised, but when PNP is added, this fraction changes to 73%. Although C=C/C-C and O-C=O in BNQDs had area percentages of 44.25% and 24.82%, respectively, they are more specifically discovered to be deconvoluted functional groups with values of 25.12% and 1.16% after the addition of PNP. While the percentages for C=O and C-O/C-N have an area of 4.45% and 15.78%, respectively, and reached after addition of PNP to 29.63% and 43.59%. After the addition of PNP, the functional group C-O-C of the BNQDs totally vanishes in C1s deconvolution. Similarly, we saw that after adding PNP in the case of O1s deconvolution, the percentages of C-O/C=O and COOH areas decreased (Table 6.4(b)). In O1s deconvolution, a new peak corresponding to the B-O bond was identified at 529.10 eV, while new deconvoluted peaks for the NO and O-O were observed at 534.63 and 530.51 eV, respectively, with area percentages of 16.76% and 4.52%.

(a)

C1s	BNQDs		PNP		BNQDs+PNP	
	Position (eV)	**% Area**	**Position (eV)**	**% Area**	**Position (eV)**	**% Area**
O-C=O	288.77	24.82	288.05	7.82	288.78	1.66
C=O	287.70	4.45	287.98	-	287.75	29.63
C-O/C-N	286.42	15.78	286.00	-	286.05	43.59
C=C/C-C	284.60	44.25	284.31	75.79	284.53	25.12
C-O-C	285.47	10.70	285.78	16.53	-	-

(b)

O1s	BNQDs		PNP		BNQDs+PNP	
	Position (eV)	**% Area**	**Position (eV)**	**% Area**	**Position (eV)**	**% Area**
NO	-	-	-	-	534.63	16.76
COOH	533.21	22.72	-	-	533.47	17.03
C-O	532.13	74.75	532.45	50.80	532.17	61.69
C=O	531.43		531.87	33.35		
B-O	529.10	2.06	-	-	-	-
O-O	-	-	530.51	15.75	530.49	4.52

Table 6. 4 (a) (b) The C1s, O1s peak positions obtained after peak fitting. The error ± 0.2 eV for peak C1s and O1s peak with PNP.

We can conclude from all these findings that PNP interacts significantly with the oxygen-containing functional groups of carbon and boron found in BNQDs. The physiosorbed on the BNQDs is visible in this interaction. As a result, the surface of functional groups on BNQDs enhances PNP interaction, strongly quenching fluorescence. TRPL study confirm the quenching processes involve as static as well as dynamic after addition of quencher. The strong interaction observed in ground and excited state after addition of quencher and get de-excited gives radiative and non-radiative emission, respectively. Hence. PL emission of as synthesized BNQDs gets quenched with the gradual addition of PNP.

6.2.5 Real sample analysis

The sensing capability of BNQDs was evaluated using real water samples containing pesticides commonly used in agriculture. The pesticides included Averest, Tabezo, Trilok, Blast, Luna,

and Regent. The photoluminescence (PL) emission spectra of these pesticides were recorded both with and without BNQDs, as shown in Figure 6.11(a, &b).

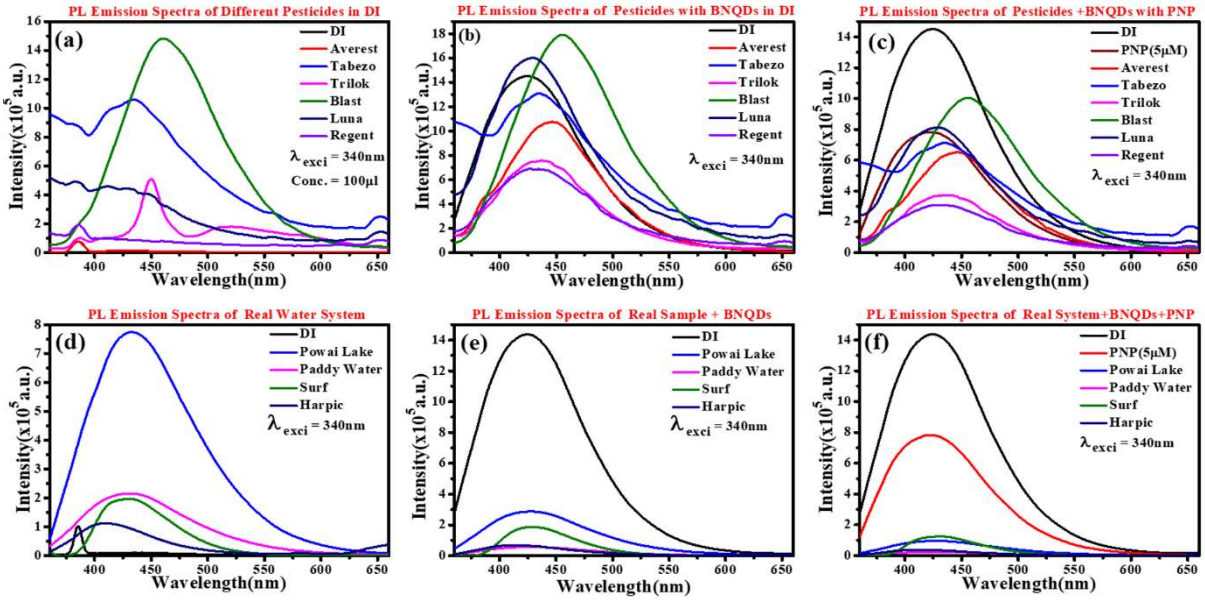

Figure 6. 11 Fluorimetry based real samples testing in pesticides and some water system using excitation as 340nm, (a) PL emission spectra of different pesticides at same concentration (100µl) in DI, (b) PL emission spectra of pesticides in the presence of BNQDs, (c) PL emission spectra of different pesticides with PNP in the presence of BNQDs, (d) PL emission spectra in the presence of real water system, (e) PL emission spectra of real water system in the presence of BNQDs, (f) PL emission spectra of real water system with PNP in the presence of BNQDs.

The results revealed that Tabezo, Averest, Triloki, and Regent exhibited PL emission quenching in the presence of BNQDs, indicating the presence of p-nitrophenol (PNP). However, Blast and Luna showed a decrease in peak intensity, likely due to the presence of fluorophores in these pesticides that emit in the same spectral region. This overlapping emission spectra poses a challenge for the detection of PNP. To address this issue, the PL emission spectra of similar molecules, including Aniline, Aminophenol, Dinitrobenzene, Methyl phenol, and Phenol, were also studied (Figure 6.12 (a-f)).

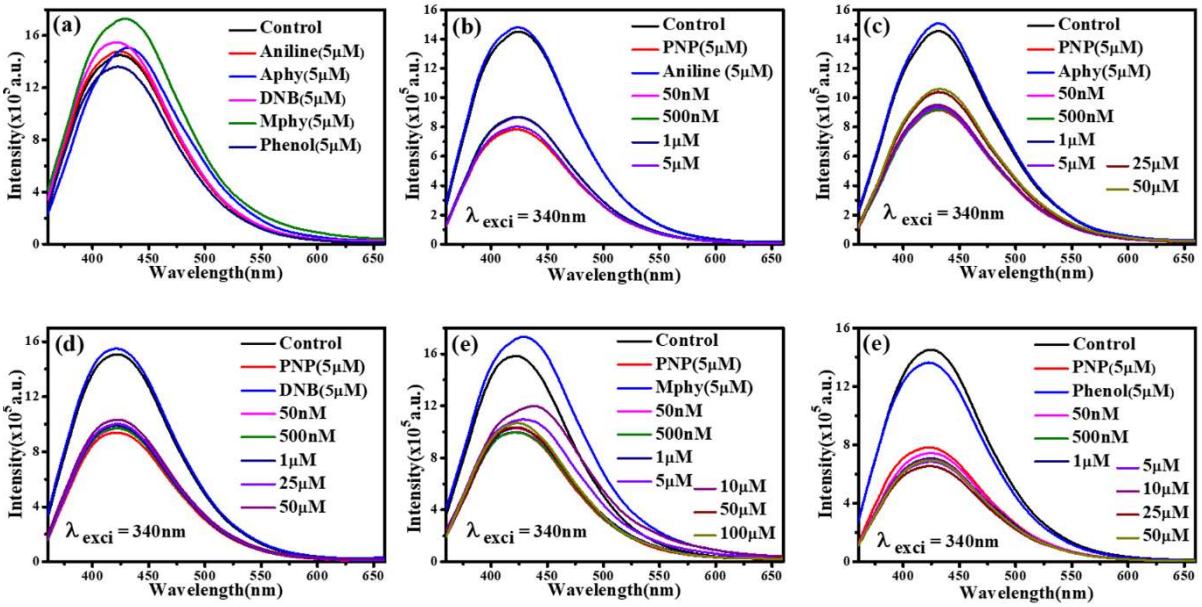

Figure 6. 12 Overlapping study of PNP with similar molecular structure molecules, (a) PL emission spectra of BNQDs with aniline, aminophenol, dinitrobenzene, methyl phenol, and phenol, (b-e) shows the overlapping PL emission spectra of PNP with aniline, aminophenol, dinitrobenzene, methyl phenol, and phenol.

The results confirmed the absence of overlapping phenomena due to similar types of molecules. These findings suggest that BNQDs have potential as a sensitive and selective detection platform for PNP in water samples contaminated with agricultural pesticides.

Figure 6.11(c) illustrated that the PL emission spectra of BNQDs with pesticides after the addition of PNP (5μM) were recorded, confirming that the decrease in PL intensity was due to the presence of PNP. To test the detection capability of BNQDs in real water samples, water samples were collected from Powai Lake, Paddy field, draining water of Surf, and Harpic, are subjected to centrifugation, filtration, and boiling to remove small particles and biological contaminations. The PL emission spectra of the real water samples in the absence of BNQDs showed emission in the emission range of BNQDs, which was attributed to the presence of other fluorescent dye molecules in these water systems[371]. However, Figure 6.11(d-f) shows the PL emission spectra in the presence of BNQDs showed quenching in the real water system

with respect to the control, confirming the presence of PNP. The PL emission spectra of the real water system in the presence of BNQDs and PNP confirmed the decreasing of PL emission due to the presence of PNP and no other similar types of molecules. The study highlights the potential of BNQDs as efficient fluorescent probes for the detection of pesticides in real water samples.

6.3 Conclusion

In this study, boron nitrate nano-powder was used as a precursor to synthesize boron nitride quantum dots (BNQDs) through hydrothermal treatment. The synthesized BNQDs were characterized using X-ray diffraction (XRD), transmission electron microscopy (TEM), and X-ray photoelectron spectroscopy (XPS) for their structural and elemental characterizations. The photophysical properties of the BNQDs were investigated using UV-Visible and photoluminescence (PL) spectroscopy. The sensing behaviour of the BNQDs towards the organic pollutant p-nitrophenol (PNP) was studied, and it was found that the BNQDs exhibited remarkable sensing behaviour with high selectivity towards PNP. The quenching constant Ka was found to be 2.325 M^{-1}, which is 14.49% of the collision quenching phenomena derived constant, indicating a defined way of quenching by the quencher towards the BNQDs PL intensity, as revealed by the modified Stern-Volmer (S-V) plot. Time-resolved PL (TRPL) studies suggest high selectivity ($Kq = 4.95x10^5 M^{-1}s^{-1}$) and sensitivity of the BNQDs towards PNP sensing. The developed probe showed a very low limit of detection (LOD) of approximately 7.91pM in a linearity range from 100pM to 1μM. Overall, this study demonstrates a cost-effective and eco-friendly approach to synthesize BNQDs, which can be used as an efficient, reliable, and feasible sensing probe for the detection of PNP in real water systems and pesticides. This study contributes to the advancement of nanomaterial-based

sensing technologies and provides insights for further development of sensing probes with high selectivity and sensitivity towards target analytes.